Sensors and Materials, Vol. 38, No. 2 (2026) 887–905
MYU Tokyo

S & M 4354

Multi-source Sensing Information-driven Flexibility and Resilience Optimization of Regional Integrated Energy Systems with Power-thermal-cold Interconnections under a Single Large Load Scenario

Shi-Hao Yin,[1] Xiao-Dong Xing,[1] Zai-He Yang,[1] Bin Zhang,[1,2*] and Ming-Liang Yang[1]

[1]Yunnan Power Dispatching and Control Center, Kunming, Yunnan Province 650500, China
[2]Faculty of Land and Resources Engineering, Kunming University of Science and Technology, Kunming 650093, China

(Received October 9, 2025; accepted December 5, 2025)

Keywords: multi-source sensing information, regional integrated energy system, multi-time-scale scheduling, multi-objective optimization, single large load

Currently, regional integrated energy systems are crucial for achieving low-carbon transformation and enhancing resilience in energy systems. In this paper, we address the challenges presented by high proportions of renewable energy integration and single large load scenarios, including temporal mismatches in multi-energy complementarity, insufficient coordination in multi-time-scale scheduling, and the complex nature of multi-objective optimization problems. First, a multi-time-scale collaborative scheduling framework for power-thermal-cold multi-energy flexible interaction under a single large load is proposed. This framework introduces a dynamic prioritization mechanism for power-thermal-cold multi-energy flows, which considers load peak-to-valley differences and energy transmission delays. Second, a collaborative scheduling strategy that integrates day-ahead forecasting, intraday rolling adjustments, and real-time feedback corrections is proposed, which is driven by multi-source sensing information. The pervasive sensor data serves as the foundation for the accurate day-ahead forecasting of renewable energy and loads, provides the basis for intraday rolling adjustments to correct forecast deviations, and enables real-time feedback control to mitigate the impact of sudden disturbances, particularly from the single large load. This closed-loop, data-driven scheduling process is central to enhancing system flexibility and resilience. Furthermore, the multi-objective optimization algorithm is improved by incorporating elite cooperation and crowded distance sorting to improve its search capabilities and convergence performance with respect to the complex "economic-low carbon-high load" Pareto frontier. Simulation results indicate that the proposed optimization strategy leads to a 9.1% reduction in operating costs for the regional integrated energy system, a 9.9% decrease in carbon emissions, and a significant 23.9% reduction in gas costs. These findings effectively validate the superiority of the proposed method in improving system economy, environmental performance, and operational resilience,

*Corresponding author: e-mail: zhangbin_ynpd@126.com
https://doi.org/10.18494/SAM5970

ISSN 0914-4935 © MYU K.K.
https://myukk.org/

providing a theoretical basis and practical solutions for the coordinated optimization of regional integrated energy systems in complex scenarios.

1. Introduction

1.1. Research background and significance

In the context of "dual carbon" goals, the Regional Integrated Energy System (RIES) plays a crucial role in the coupling of electricity, cooling, and heating, which facilitates the integration of renewable energy and reduces carbon emissions.[1,2] By incorporating distributed photovoltaics, wind power, and other renewable sources, along with energy storage and diverse loads such as cooling and multi-type demands, RIES enhances system flexibility. However, as application scenarios expand, challenges in IES development are intensified by factors such as extreme weather, the high penetration of renewable generation, and the integration of multiple entities. These challenges include incomplete resilience assessment, discontinuous time-scale modeling, and difficulties in accurately representing large single-category loads.[3,4] Li *et al.* argued that unplanned electric vehicle (EV) charging, for instance, leads to overlapping residential and EV load peaks, increasing the grid peak-to-valley difference by more than 30%.[5] Moreover, owing to the coupling characteristics of heating and cooling energy, conventional IES models are inadequate for a multi-energy coupled regional IES.[6]

1.2. Literature review

Existing studies on resilience and coordination in distribution networks and RIES have notable limitations. Dwivedi *et al.* improved the resilience of the Institute of Electrical and Electronics Engineers 123-node system from 56 to 93% by incorporating complex network topology and electrical parameters but did not consider multi-energy complementarity or multi-time-scale correction in IES.[1] Liu *et al.* used a three-stage stochastic robust approach to enhance RIES robustness but overlooked scenarios with large single loads and significant peak-valley differences.[2] Chen and Li developed a super-network model integrating fossil fuel networks with transport networks and introduced variational inequalities for dispatch path adjustment, yet they ignored renewable energy contributions, multi-energy storage, and real-time sensor feedback.[3] Jin *et al.* enhanced electricity-thermal coordination accuracy by increasing source-side output but failed to account for the dynamics and real-time feedback of cooling networks.[4] Li *et al.* proposed an enhanced temporal convolutional network-bidirectional long short-term memory prediction model combined with a three-stage control short-term energy storage approach to reduce overlap between EV charging and residential loads, achieving a 27% reduction in load overlap and PV curtailment,[5] but this approach was criticized for neglecting heating-cooling energy coordination. Li *et al.* pointed out that conventional models fail to account for thermal and cooling energy storage losses, resulting in overestimated capacity evaluations.[7] Wang *et al.* indicated that maintenance protocols neglect the inspection and repair of heat pumps and chillers, leading to increased failure rates.[8] Both Li *et al.* and Wang *et al.*

pointed out that conventional models fail to account for thermal and cooling energy storage losses, resulting in overestimated capacity evaluations. Fathy developed a Superb Fairy-wren Optimization Algorithms (SFOA) model to address uncertainties in multi-energy microgrids, using Beta/Weibull distributions to quantify renewable energy fluctuations and reducing EV scheduling costs by 17.28% through demand response,[9] but it remains limited to microgrid scheduling and lacks multi-energy, multi-time-scale IES integration.

Existing studies on RIES collaborative optimization face challenges in scenario matching and scheduling precision. Lu *et al.* developed a bi-level optimization model for community IES, achieving a 9.6% cost reduction by optimizing energy procurement, storage, and equipment output.[10] However, it neglected cooling systems, inter-community trading, and the concentrated demand characteristics of large single loads. Wu *et al.* adopted a cooperative game approach to balance stakeholder benefits in multi-stakeholder scheduling but failed to quantify the impact of thermal/cooling energy transport delays.[11] Wang *et al.* implemented categorized energy demand scheduling to reduce carbon emissions by 16.8% across industrial, commercial, and residential scenarios but did not emphasize the high response speed required by large single loads.[12] Li *et al.* proposed a day-ahead, intra-day, and real-time scheduling framework to balance energy supply and demand but ignored the priority of multi-energy complementarity.[13] Wang *et al.* employed flow response superposition to decompose flow demand but lacked real-time sensor feedback for dynamic accuracy.[14] Liu *et al.* introduced a bi-level game model to reduce operational costs through multi-agent coordination but showed limited applicability to large single loads. Overall, these studies exhibit gaps in comprehensive scenario integration and precise scheduling mechanisms.

In summary, existing studies generally lack integrated approaches for multi-energy complementarity across multiple time scales, effective strategies for large single loads, and the fusion of multi-agent and sensor feedback, hindering the coordinated management of large single loads within a multi-energy, multi-time-scale framework.

1.3. Innovation and contributions

Current RIES research has explored multi-time-scale scheduling and multi-energy complementarity, but challenges remain in handling complex scenarios with varying renewable energy integration and large singular loads. Most studies lack targeted strategies for sudden large load impacts during extreme weather, and improvements are needed in algorithm convergence and solution quality for high-dimensional nonlinear multi-objective optimization problems. In this paper, we address these issues with the following innovations and contributions:

- A multi-source sensing information-driven collaborative scheduling framework for electricity, thermal, and cold under large load scenarios is proposed. This framework relies on real-time sensor data to accurately assess the supply-demand status and identify critical bottlenecks. The dynamic priority sorting and cross-energy support mechanisms are activated and guided by this continuous sensor feedback, enabling proactive load shifting and enhancing resilience to balance supply and demand in extreme cases.
- The multi-objective great wall construction algorithm (MGWCA) is improved with elite collaborative optimization and crowding distance sorting, balancing global exploration and

local development to efficiently solve high-dimensional nonlinear multi-objective problems.

- A bi-level scheduling optimization model based on MGWCA is constructed to enable collaborative decision-making among stakeholders. Case studies validate its effectiveness in reducing costs, minimizing emissions, and enhancing extreme load response capabilities.

The following sections are organized as follows. In Sect. 2, we build the RIES framework and discuss multi-time-scale scheduling. MGWCA improvements are described in detail in Sect. 3. Section 4 covers bi-level scheduling. In Sect. 5, we validate the framework via case studies. Findings and limitations are summarized in Sect. 6.

2. Formulation of Multi-source Sensing Information-driven Flexibility and Resilience Optimization Model of Regional Integrated Energy System

2.1 Multi-source sensing information-driven structural framework of RIES

RIES operates on the basis of user energy demands. Sensors collect real-time data on energy supply, demand, and equipment status. This coordination integrates renewable energy (wind and solar) with traditional sources (gas turbines and boilers) to meet diverse loads (electricity, heating, and cooling). Energy storage devices mitigate renewable fluctuations and optimize distribution. The system involves three main participants: energy producers, energy managers, and the RIES itself. Managers purchase energy from producers, set real-time pricing, and distribute it downstream. Bidirectional collaboration with external grids ensures supply during shortfalls and allows surplus energy feedback, enhancing reliability and efficiency. Figure 1 shows the optimization framework of RIES.

The real-time operation of RIES depends on a sensor network at critical nodes in energy production, conversion, storage, and end-user load sectors. The network includes four types of sensing node: environmental nodes (monitoring wind speed, sunlight, temperature, and humidity), electrical nodes (measuring voltage, current, and power), thermal nodes (monitoring temperature, flow rate, and pressure), and status nodes (tracking equipment states and faults). The sampling period for all sensors is uniformly set at Δt = 5 min to meet optimization requirements. The general sensor model is

$$\begin{cases} \hat{y}_{k,t} = y_{k,t} + \chi_{k,t}^{bias} + \chi_{k,t}^{noise}, \\ \chi_{k,t}^{bias} = \alpha_k \cdot y_{k,t}, \\ \chi_{k,t}^{noise} \in \mathrm{N}(0, \sigma_k^2), \end{cases} \tag{1}$$

where $\hat{y}_{k,t}$ is the measured value transmitted by the sensor, $y_{k,t}$ is the true value of the physical quantity being measured, $\chi_{k,t}^{bias}$ indicates the system bias, $\chi_{k,t}^{noise}$ represents random noise, and α_k signifies the relative deviation coefficient.

The accuracy requirements for sensor data necessitate the quantification and correction of measurement errors by introducing parameters such as systematic bias, random noise, and relative deviation coefficients. The real-time requirements stipulate a unified sampling period of

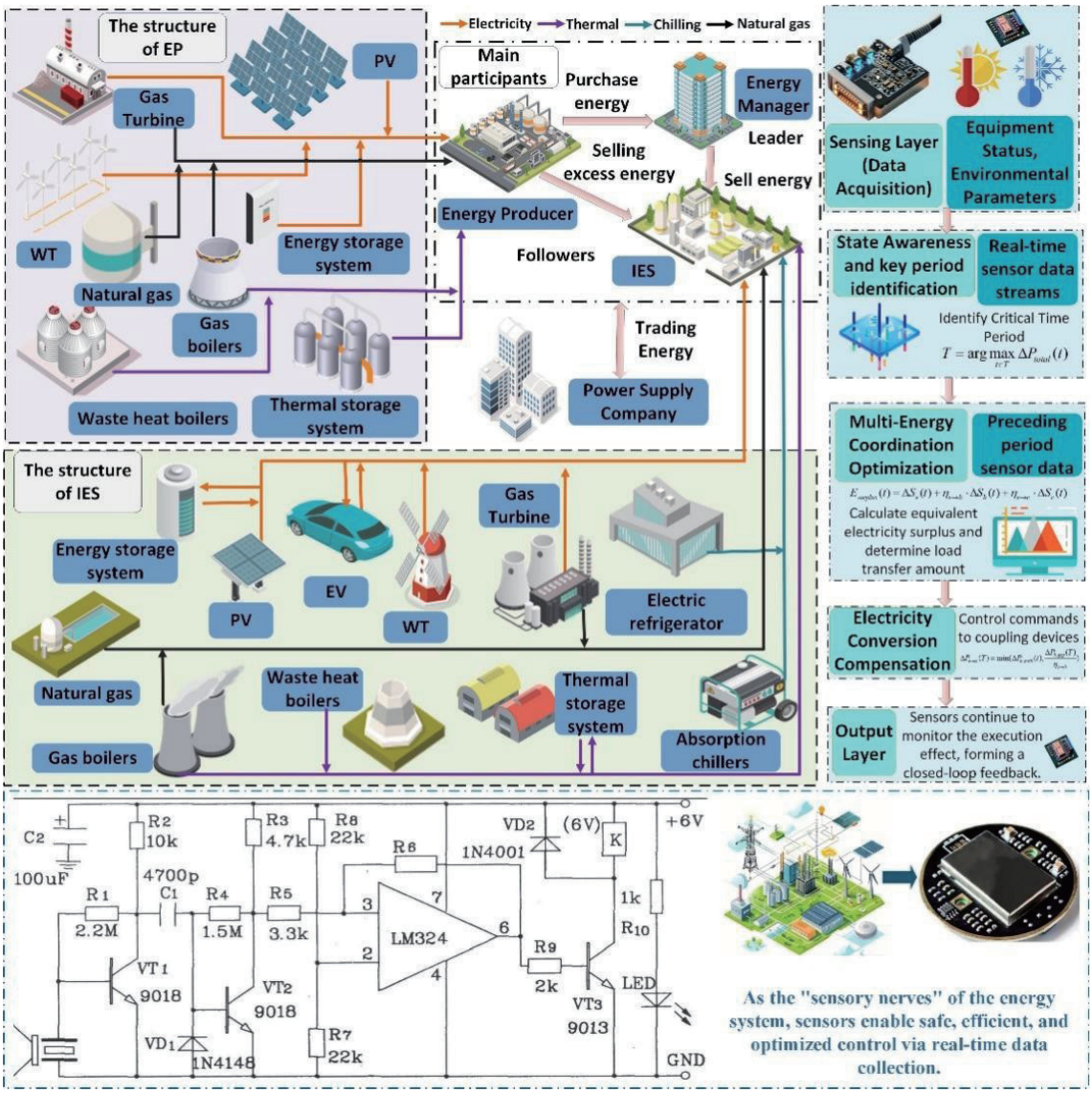

Fig. 1. (Color online) Framework diagram of multi-source sensing information-driven RIES.

Δt = 5 min for all sensors in the system, enabling the capture of rapid and stochastic fluctuations in renewable energy output (such as photovoltaic and wind power) and various loads. The combination of the unified Δt = 5-min sampling cycle and accuracy requirements collectively forms the "sensory neural network" of the regional integrated energy system. By integrating high-precision, real-time multi-source sensing data, the regional integrated energy system achieves dynamic, responsive, and adaptive operational capabilities, laying the foundation for flexibility and resilience optimization in complex scenarios such as single large loads and the high penetration of renewable energy integration.

2.2 Mathematical model for RIES

The top-level model of the RIES developed in this study integrates key components such as renewable energy sources, combined heat and power (CHP) systems, multi-energy coupling conversions, and energy storage, through the mathematical modeling of energy production, conversion, storage, and load segments.

The equipment in the integrated energy system includes photovoltaic panels, wind turbines, gas turbines, and electric chillers. The equipment modeling is described in detail in Ref. (15). The revenue from energy sales and operational costs comprise the objective function for energy producers, while the objective function for energy managers includes only the profits from electricity trading.[16]

The electrical balance constraint model for IES is

$$\begin{aligned} &D_{W1}(t) + D_{W2}(t) + D_{W3}(t) + D_{W4}(t) + D_{W5}(t) + D_{W7}^{aisc}(t) \\ &= D_{LOAD}(t) + D_{EV-MOV}(t) + D_{SOC}(t) + D_{cc}(t), \end{aligned} \tag{2}$$

where $D_{W1}(t)$ is the wind power generation, $D_{W2}(t)$ denotes the PV power generation, $D_{W3}(t)$ indicates the power output from GT, $D_{W5}(t)$ is the amount of electricity purchased from energy managers, $D_{W7}^{disc}(t)$ is the discharge quantity, $D_{LOAD}(t)$ signifies the electrical load demand, $D_{EV-MOV}(t)$ indicates the amount of transferred electricity, and $D_{cc}(t)$ is the power consumption of the carbon capture system.

The thermal load balance constraint model for IES is

$$E_B^G(t) + E_R^H(t) + E_{BUY}(t) + E_L(t) = E_{LOAD}(t) + E_{CHAR}(t), \tag{3}$$

where $E_{LOAD}(t)$ is the thermal load demand, $E_B^G(t)$ is the power output of the gas boiler, $E_{BUY}(t)$ is the quantity of heat purchased, $E_R^H(t)$ is the power output of the heat recovery boiler.

The cold load balance constraint for IES is

$$C_O^L(t) + C_E^Q(t) = C_O^D(t), \tag{4}$$

where $C_O^L(t)$ is the cooling power of the absorption chiller, $C_E^Q(t)$ denotes the cooling power produced by the electric chiller, and $C_O^D(t)$ indicates the total demand for cooling load.

The power balance constraint for energy producers is

$$\begin{cases} E_{EP}(t) + E_{PV}^{EP}(t) + E_{GT}^{EP}(t) + E_{DISC}^{EP}(t) = E_{SELL}^{EP} + E_C^{EP} + E_{SW}^{EP}, \\ P_{EP}^{GT}(t) + P_{EP}^{DISC}(t) = P_{EP}^{SELL}(t) + P_{EP}^{C}(t) + P_{EP}^{SW}(t), \end{cases} \tag{5}$$

where $E_{EP}(t)$, $E_{PV}^{EP}(t)$, and $E_{GT}^{EP}(t)$ represent the power outputs of GWT, PV, and GT, respectively. $E_{DISC}^{EP}(t)$ and E_C^{EP} denote the discharge and charge capacities of the energy storage devices,

respectively. E_{SW}^{EP} indicates the amount of electricity fed into the grid, $P_{EP}^{GT}(t)$ represents the amount of heat generated by GT and processed through the heat recovery boiler, and $P_{EP}^{DISC}(t)$ and $P_{EP}^{C}(t)$ signify the amount of heat released and stored by the thermal storage devices, respectively, with $P_{EP}^{SW}(t)$ specifically denoting the amount of heat sold.

The energy management provider (EMP) acts as a "mediator" between energy producers and the integrated energy system. The constraints applicable to the EMP, as related to energy producers and the integrated energy system (including electrical transmission lines and thermal networks), are described in Ref. (16)

2.3 Multi-time-scale collaborative scheduling framework for power-thermal-cold multi-energy flexible interaction under a single large load

Under extreme weather and large single-load integration, regional integrated energy systems face significant operational challenges. Traditional load scheduling methods, limited to a single energy form, are inadequate for addressing large-scale power deficits. In this paper, we propose a multi-time-scale collaborative scheduling framework for power-thermal-cold multi-energy flexible interaction. The strategy integrates various energy flows, leveraging the spatiotemporal transfer potential and complementary characteristics of electrical, thermal, and cooling loads to enhance system resilience and economic efficiency under extreme conditions.

The implementation of this strategy relies on the accurate assessment of the overall supply-demand situation and the identification of critical bottlenecks. An integrated model of joint deficits for electricity, thermal , and cooling loads is essential to fully capture system pressures. This model reflects the absolute deficits of each energy subsystem and introduces weighting factors to account for differences in scheduling priorities, conversion costs, and reliability requirements of various energy sources.

$$\Delta P_{total}(t) = \alpha_e \cdot \max(0, P_e^d(t) - P_e^s(t)) + \alpha_h \cdot \max(0, P_h^d(t) - P_h^s(t)) + \alpha_c \cdot \max(0, P_c^d(t) - P_c^s(t)) \quad (6)$$

Here, $\Delta P_{total}(t)$ is the weighted total load deficit; α_e, α_h, and α_c denote the weighting coefficients for electricity, thermal, and cooling, respectively. $P.^d$ and $P.^s$ represent the demand and supply capacities for electricity, thermal, and cooling, respectively.

On the basis of this model, the maximum joint deficit of the system at time T can be determined through the optimization model:

$$T = \arg\max_{t \in T} \Delta P_{total}(t). \quad (7)$$

Moment T represents the most vulnerable point in the system during the scheduling period and is the target that the cooperative scheduling strategy aims to stabilize. Once the critical time point T is identified, the core of the strategy is to use resources from preceding time periods for "proactive" load shifting. This approach leverages the inertial characteristics and energy storage potential of thermodynamic systems, allowing thermal and cooling energy to be transferred and stored over time at a relatively low cost.

To achieve unified scheduling across different energy sources, it is necessary to convert the surplus energy for electricity, thermal, and cooling at all times ($t < T$) into a comparable baseline value. In this paper, the "equivalent electrical energy surplus" at time t is defined as

$$E_{surplus}(t) = \Delta S_e(t) + \eta_{e\to h} \cdot \Delta S_h(t) + \eta_{e\to c} \cdot \Delta S_c(t), \tag{8}$$

where $E_{surplus}(t)$ is the equivalent electrical energy surplus, and $\Delta S.(t)$ denotes the net surplus of each energy type. The coefficients $\eta_{e\to h}$ and $\eta_{e\to c}$ represent the conversion efficiencies from electrical energy to thermal and cooling energy, respectively, facilitating the homogeneous treatment of diverse energy sources within the scheduling decision-making process.

To prevent new supply–demand imbalances in preceding time periods, load transfer amounts must follow principles of systemic balance and proportionality. The amount of load transferred from time t to the critical moment T is determined as

$$\Delta P_{transfer}(t,T) = \min\left(E_{surplus}(t), \frac{\Delta P_{total}(T) \cdot E_{surplus}(t)}{\sum_{t=1}^{T-1} E_{surplus}(t) \cdot \varphi^{(T-t)}} \right), \tag{9}$$

where $\Delta P_{transfer}$ is the amount of load transferred and φ is the energy storage loss coefficient. This allocation mechanism ensures that the transferred load in each time period is proportional to its energy buffer, thereby optimizing the allocation of system resources over time while distributing risk.

To address insufficient self-regulation capacity in a single energy subsystem during extreme scenarios (e.g., large load integration), in this strategy, we introduce a deeper cross-energy complementarity mechanism. When the thermal (or cooling) load deficit at time T exceeds the capacity of its own energy storage and transfer, an unresolvable power gap emerges. In such cases, the highly controllable electrical energy system acts as a critical flexible resource, providing support through energy conversion devices such as CHP units, heat pumps, and electric chillers.

To realize this complementary process, the remaining flexibility after meeting electrical scheduling demands must first be determined. Then, electrical energy can be converted into thermal or cooling energy via coupling devices. The amount of conversion is constrained by available electrical power, conversion efficiency, and the actual demand gap, as defined by

$$\Delta P_{e\to h}(T) = \min\left(\Delta P_{e,avail}(t), \frac{\Delta P_{h,gap}(T)}{\eta_{e\to h}} \right), \tag{10}$$

where $\Delta P_{e,avail}$ is the remaining flexibility that can be utilized after meeting the scheduling demands for electrical energy and $\Delta P_{h,gap}$ denotes an unresolvable power gap. This mechanism essentially establishes a bidirectional mutual support network among the electrical, thermal, and cooling subsystems. When one subsystem experiences extreme pressure, the other subsystems can provide effective flexibility support, thereby significantly enhancing the overall robustness of the integrated energy system.

The proposed cooperative scheduling strategy is a systematic approach with hierarchical levels and responsive actions. It includes global state awareness to identify critical periods, multi-energy coordinated optimization for load transfer based on equivalent surpluses, and cross-subsystem mutual support through electrical energy conversion when needed. This forms a comprehensive scheduling defense system for extreme load scenarios. Its theoretical value lies in extending load flexibility from the temporal to the energy category dimension, offering an innovative solution for the efficient, safe, and economical operation of integrated energy systems. Future research will focus on developing stochastic optimization models and distributed solving algorithms for this strategy under uncertain environments. Figure 2 shows the framework of the proposed strategy.

3. Muit Great Wall Construction Algorithm (MGWCA)-based Solving Method

In RIES scheduling, the coupling of multi-energy flows and source-load uncertainties introduces significant dynamic disturbances and solution complexity. Traditional optimization algorithms such as the genetic algorithm often struggle with high-dimensional, strongly nonlinear, and multi-objective problems. The great wall construction algorithm (GWCA), inspired by the hierarchical logic and collaborative defense mechanisms of the great wall's construction, demonstrates strong robustness, high search accuracy, and a lower risk of being trapped in local optima, making it well suited for multi-objective optimization in complex energy systems. The mathematical model of GWCA is described in detail in Ref. (17).

In the original GWCA, the labor movement form is fixed, which can lead to the premature convergence of the population, and the algorithm lacks effective global exploration. To address these shortcomings and enhance the adaptability of the solution model, an elite collaborative optimization strategy is proposed to update the position of labor, as defined by

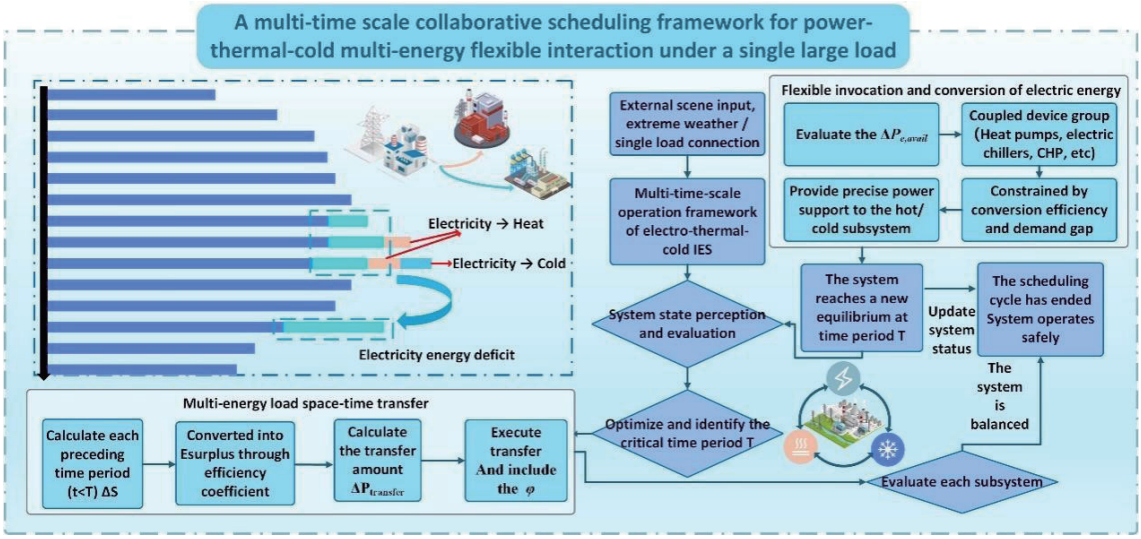

Fig. 2. (Color online) Framework diagram of the proposed strategy.

$$\begin{cases} elite = w_1 * (v_i(t) - L_i(t)), \\ mry = w_2 * (L_{best}(t) - L_i(t)), \end{cases} \tag{11}$$

$$L_i(t+1) = L_i(t) + elite * rand(1, dim) + mry, \tag{12}$$

where *elite* is the elite guiding component, *mry* denotes the individual memory component, and w_1 and w_2 are the guiding weights for the elite and individual memory, respectively. $L_i(t)$ is the position of the i_{th} laborer, and $L_{best}(t)$ refers to the best position of the laborer. $v_i(t)$ signifies the position of the i_{th} engineer, $L_i(t + 1)$ is the position of the i_{th} laborer, and *dim* denotes the dimensionality of the problem.

The elite collaborative optimization strategy balances global search and local development capabilities, significantly improving convergence speed. On this basis, MGWCA incorporates crowded distance sorting and an external archiving mechanism. The detalis of the multi-objective optimization process are shown in Ref. (16).

The framework diagram of MGWCA is shown in Fig. 3. First, set the algorithm parameters and the basic parameters of the repository, then calculate the initial fitness values of all

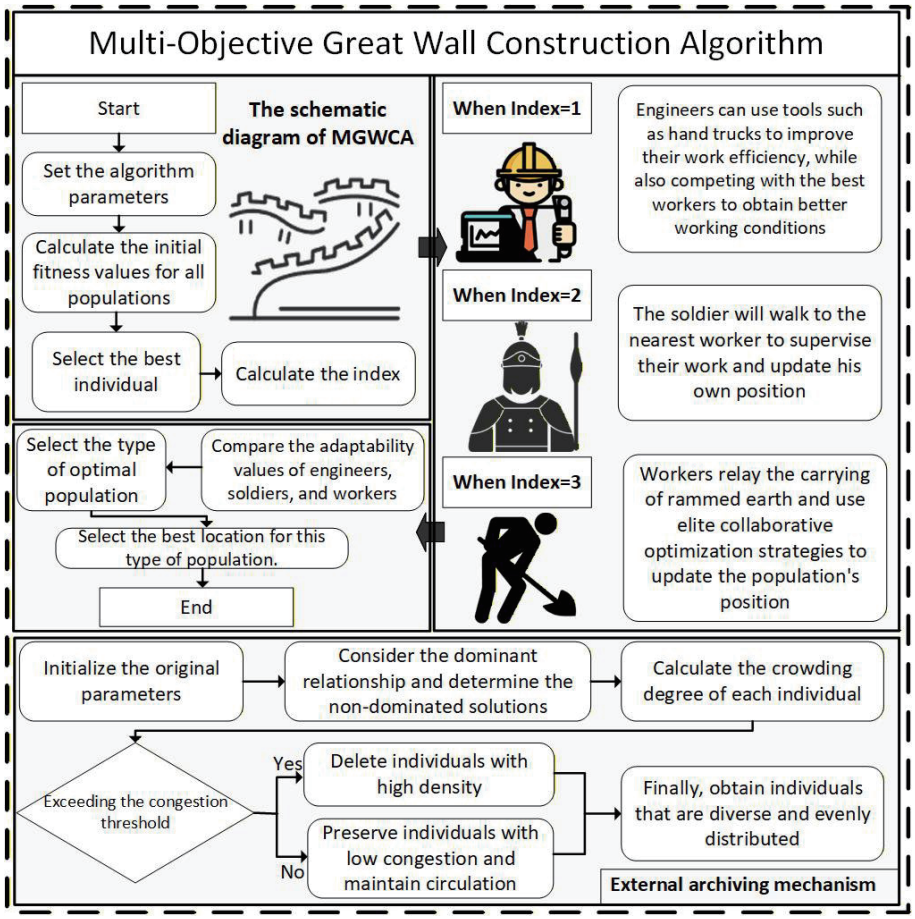

Fig. 3. (Color online) Framework diagram of MGWCA.

populations, and, finally, select the best individual as the leader to guide the population individuals to move towards its position. Next, calculate the index. When the index is 1, the population updates positions using the engineer's method; when it is 2, the soldier's method is used; and when it is 3, the worker's method is applied. After the population update, compare the fitness values of engineers, soldiers, and workers, select the population position corresponding to the optimal fitness value, and store it in the repository. This process is repeated until the maximum number of iterations is reached. If the repository becomes full, priority is given to individuals with lower densities and higher fitness values. Finally, the best individual is selected from the repository as the optimal solution.

4. Optimization Process of Multi-source Sensing Information-driven Flexibility and Resilience Optimization Model of RIES

The process is shown in Fig. 4. In RIES, stakeholders have different goals: energy producers balance trading revenue and costs to maximize benefits, energy managers focus on trading profits, and the integrated energy system aims to minimize comprehensive costs (trading, operations, and collaborative optimization). The system uses a bi-level framework: the upper

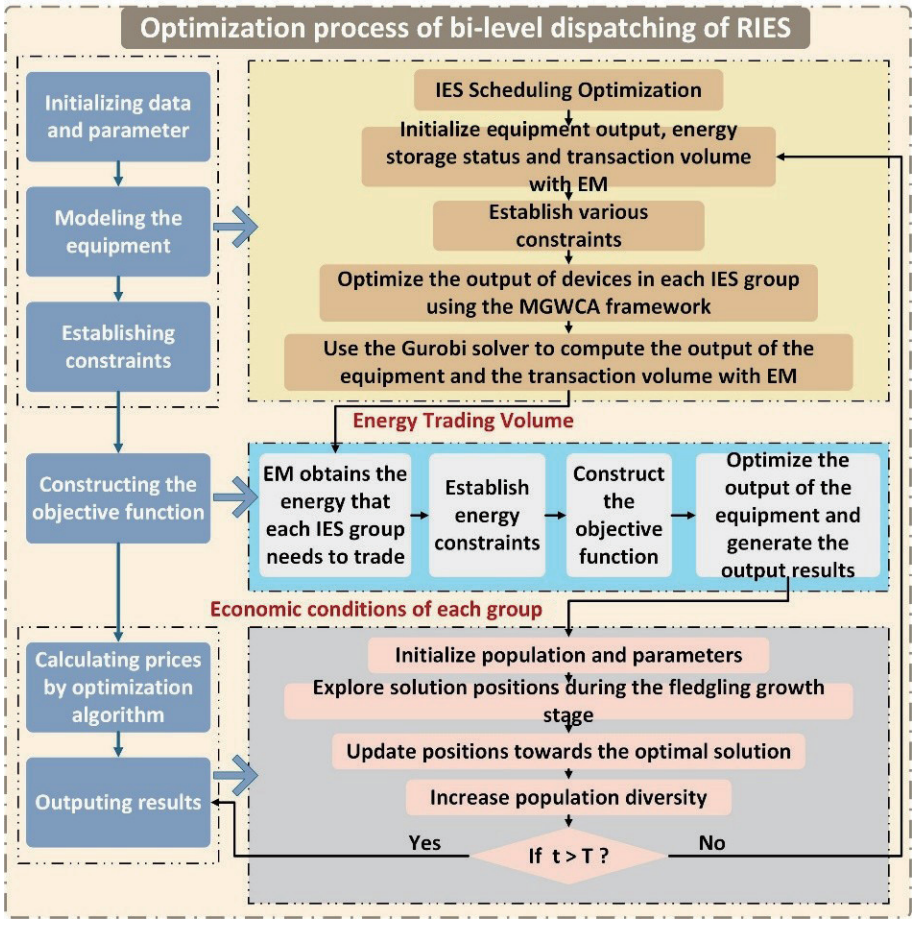

Fig. 4. (Color online) Bi-level energy optimization process of RIES.

level sets trading rules via dynamic pricing by producers and managers, whereas the lower level handles equipment scheduling and collaborative operations. Implementation includes publishing dynamic prices, initial output optimization using mixed-integer linear programming, secondary energy interactions via distributed optimization, producers adjusting output plans with linear programming, and managers settling economic returns. The model is solved using a hybrid strategy: upper-level optimization with MGWCA for pricing parameters and lower-level optimization with the Gurobi solver. As presented in Fig. 4, the specific solution process is as follows:

(1) The main program is initiated, completing the overall initialization, which includes data and parameter settings, as well as establishing the corresponding device models for the integrated energy system.
(2) Initial values are assigned to key variables, including equipment output power and trading quantities with the energy manager.
(3) Multiple operational constraints are set, encompassing power balance, output ranges for equipment, ramping capabilities, and capacity restrictions.
(4) An optimized scheduling of the equipment output within the integrated energy system is performed. The Gurobi solver is called to calculate the specific output of each device and trading quantities with the energy manager. Optimization results are then outputted to provide data support for strategic adjustments at the upper level.
(5) In constructing the optimization objective function for the integrated energy system, multiple factors such as energy costs, equipment operating expenses, and environmental benefits are comprehensively considered to achieve the economic operation of the system.
(6) Additionally, the objective function is dynamically adjusted on the basis of feedback information from the lower tier to ensure the accuracy and adaptability of the optimization process.
(7) By employing MGWCA, the optimal output of each device within the system and the corresponding trading quantities with the energy manager are derived, thereby achieving the efficient economic operation of the integrated energy system and optimizing resource allocation.

5. Case Studies

To evaluate the effectiveness of the algorithms and strategies proposed in this study, three case studies have been designed as follows: Case 1 integrates MGWCA into RIES and compares its solving capacity and superiority against SFOA, the Multi-objective Multi-verse Optimizer (MOMVO) algorithm, and the original algorithm. Case 2 verifies the flexible electricity-thermal-cold collaborative strategy through a comparison of scenarios with high and medium shares of renewable energy. Case 3 assesses the overall performance of the integrated energy system, aiming to analyze the multi-energy flexibility between electricity, thermal, and cooling, and validates the effectiveness of the multi-time-scale collaborative scheduling strategy under extreme load conditions.

The key parameters for the core equipment within RIES (such as photovoltaic panels, wind turbines, gas turbines, combined heat and power systems, energy storage devices, and energy conversion units), along with the associated cost coefficients and technical constraints, are described in detail in Appendix A.

5.1. Case 1: Numerical and solving model validation of MGWCA

To verify the feasibility of MGWCA discussed in this paper, we selected two multi-objective algorithms: SFOA and MOMVO, along with the unmodified original GWCA for comparative analysis. The iterative relationship between the optimization results and the revenues of the three major operators under different algorithms are presented in Fig. 5.

Figure 5(a) presents the optimal solutions during the iterations of the four algorithms. Notably, MOMVO records an EM loss of $−3382, while SFOA reports an EM revenue of $7123, both of which are illogical results. In contrast, MGWCA shows the lowest IES cost at $882.2, demonstrating reductions of 51.93, 38.09, and 38.65% compared with the IES costs of SFOA, GWCA, and MOMVO, respectively. This indicates a significant advantage of MGWCA in reducing IES costs. Simultaneously, the EP cost for MGWCA is $15530, which is 0.13% higher than that of GWCA, suggesting that MGWCA slightly improves the EP revenue compared with the original algorithm. Overall, under the multi-time-scale collaborative framework of multi-energy flexibility at a single high load, MGWCA showcases superiority in both reducing IES costs and enhancing the EP revenue.

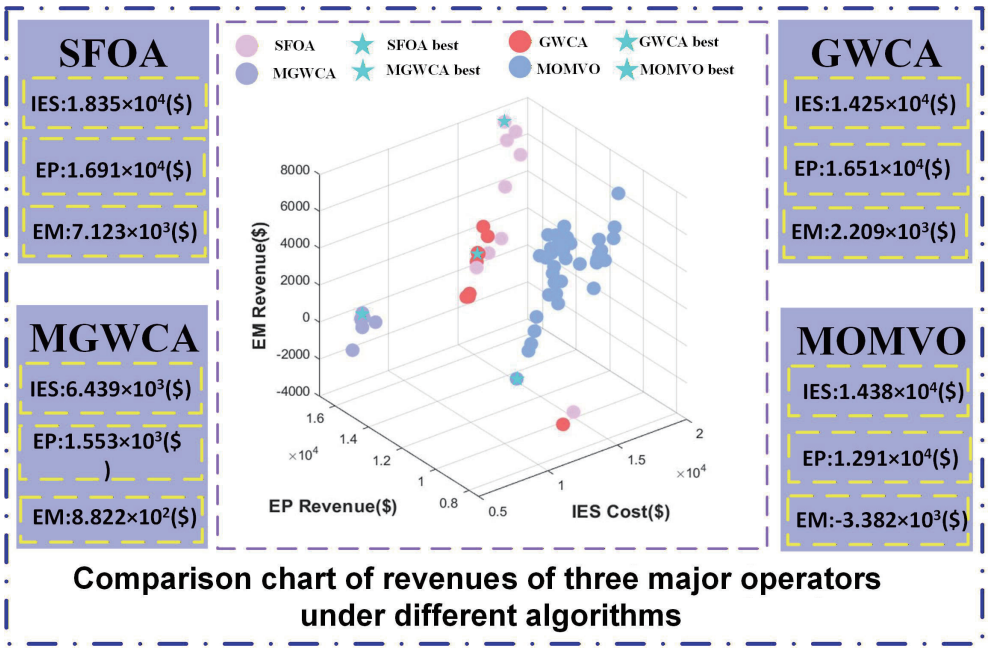

Fig. 5. (Color online) Iterative relationship between optimization results and revenues of three major operators under different algorithms.

5.2 Case 2: Feasibility verification of load scheduling strategies under different proportions of renewable energy

Case 2 validates the flexible electricity-thermal-cold collaborative strategy by comparing scenarios with high and medium shares of renewable energy. The findings indicate that this strategy effectively transforms the temporal and spatial mismatch of "green electricity and waste heat" into a layered defense of "energy storage and external procurement", ensuring that IES operates economically and resiliently under any proportion of green electricity.

Figure 6 reveals the energy balance under a high proportion of renewable energy integration. Figure 6(a) shows the electrical balance within 24 h: at 18:00, the load dropped sharply by 1048.48 kW and the remaining power was prioritized for storage in the battery. From 10:00 to 15:00, the peak output of photovoltaic power was 3116.389 kW, combined with 987.102 kW of wind power. The total power generation was much higher than the load. The system immediately initiated the "cross-energy compensation" decision - when the real-time electricity price was less than 0.35 $/kWh and the storage SOC was greater than 80%, it was determined as "surplus electricity". According to the measured efficiency curves of $\eta_{e\to h}$ = 0.9 (weighted by electric boiler +COP 3.0 heat pump) and $\eta_{e\to c}$ = 0.7 (COP 4.0 of the electric chiller and taking into account the loss of the refrigerant pipeline), the excess electricity was respectively converted into hot water and chilled water. The hot water was stored in the 85 °C storage tank and the chilled water was stored in the 7 °C cold storage tank. From 00:00 to 04:00, when the heat tank was fully filled, heat was sold to the outside. From 09:00 to 13:00, the surplus electricity from the photovoltaic system was used for heating or cooling and sold externally. At 14:00, when the heat tank dropped to 30%, the gas boiler was triggered to replenish heat. At 19:00, when the peak heat load was 769.891 kW and the heat tank was still insufficient, the heat pump was called first in the "electricity-heat priority order" and then natural gas was purchased. This strategy realizes the horizontal complementarity of "electricity-thermal-cold", convert the time deviation of renewable energy into the energy sales revenue, and enhance economic efficiency and flexibility.

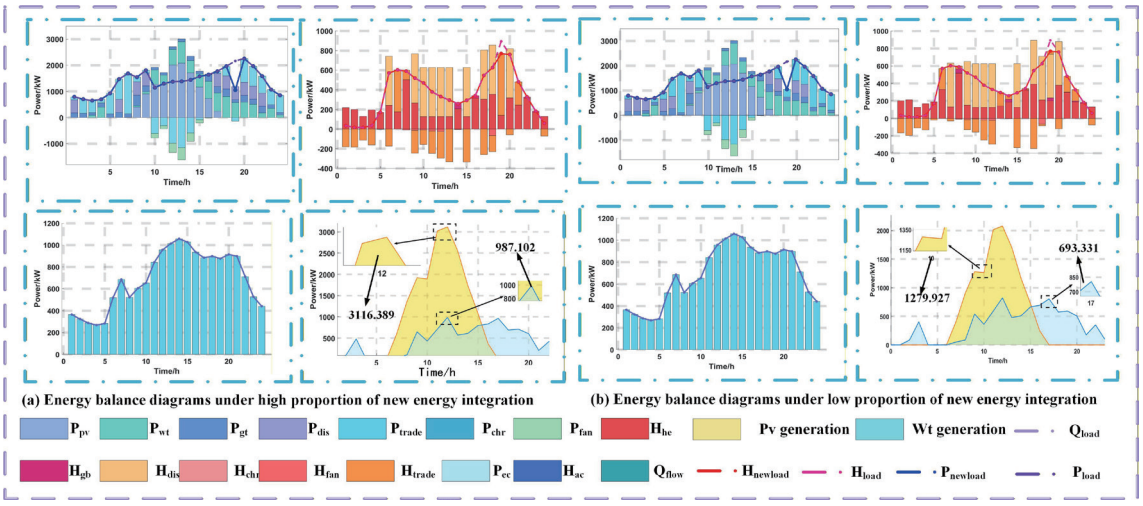

Fig. 6. (Color online) Energy balance under high and low proportions of renewable energy integration.

Figure 6(b) shows the low-renewable scenario: at 22:00, the wind and solar power output was only 329.821 kW. The system determined that the electricity price was greater than 0.65 $/kWh and the electricity shortage was greater than 1 MW. It immediately shut down the electric boiler and electric refrigeration machine, stopped the conversion from electricity to heat or electricity to cold, and released 544.825 kW of pre-stored electricity and purchased 1250.85 kW of electricity. At 13:00, the heat tank was at 25% and there was no electricity surplus. Therefore, according to the rule "purchase 151.964 kW of heat when the heat shortage is greater than 150 kW", 151.964 kW of heat was purchased to avoid inefficient electricity-to-heat conversion. The total photovoltaic power was 2077.59 kW and the wind power was 693.331 kW, which were 1038.79 and 293.771 kW lower than the high-renewable scenario, respectively. However, the cross-compensation logic of "efficient conversion when there is excess electricity and stopping conversion when there is insufficient electricity" maintained the energy supply balance, verifying the robustness and universality of $\eta_{e\to h}$ and $\eta_{e\to c}$ based on the measured efficiency of the equipment for the system under different renewable penetration rates.

In conclusion, Case 2 achieved flexible load transfer and multi-energy coordination by dynamically determining the timing of "electricity-to-thermal or electricity-to-cool" conversion and using measured efficiency values. This significantly enhanced the economic efficiency and flexibility of RIES under extreme load and renewable fluctuation conditions.

5.3 Case 3: Validation of the effectiveness of multi-energy flexibility in multi-time-scale cooperative scheduling

Case 3 aims to evaluate the overall performance of the integrated energy system, analyzing the multi-energy flexibility between electricity, thermal, and cooling. This case seeks to validate the effectiveness of the multi-time-scale cooperative scheduling strategy under extreme load conditions. As shown in Table 1, a comparative analysis is conducted on various indicators, including economic costs, pollution penalty costs, operational and maintenance costs, gas costs, and carbon emissions for IES and EP before and after cooperative scheduling.

As shown in Table 1, the implementation of multi-energy flexibility and multi-time-scale cooperative scheduling for electricity, thermal, and cooling in IES has led to significant improvements in economic and environmental performance. The economic cost of IES decreased from $2723.32 to $474.34 (a reduction of approximately 9.1%), while carbon emissions dropped from 2744.57 to 2472.31 kg (a decline of 9.9%). Gas consumption and costs also

Table 1
Various indicators of IES and EP before and after collaborative scheduling.

Objective	IES	IES after collaboration	EP	EP after collaboration
Feco ($)	2723.32	2474.34	14443.94	14340.43
Fpoll ($)	507.26	505.69	299.17	250.13
Fom ($)	1232.21	1210.59	236.06	185.95
Fgas ($)	974.12	741.15	782.69	692.30
Qec (kg)	686.94	694.12	411.52	382.15
Pec (kg)	228.98	230.53	198.04	204.73
carbon (kg)	2744.57	2472.31	1881.06	1705.34

decreased, with gas costs falling from $974.12 to $741.15 (a reduction of about 23.9%). The electricity consumption of the IES's electric chiller increased slightly from 228.98 to 230.53 kg (0.7%), whereas its cooling output decreased from 686.94 to 649.12 kg (5.5%), indicating stable power output and reliable cooling support. For EP, the economic cost decreased from $14443.94 to $14340.43, operational and maintenance costs dropped from $236.06 to $185.95, carbon emissions fell by 9.3%, and pollution costs decreased by 16.4%. These results demonstrate that the scheduling strategy optimizes the energy structure, enhances low-carbon operations, and improves the overall resilience and collaborative efficiency of IES and EP, achieving a dual win in economic viability and environmental friendliness.

Figure 7 presents the energy storage equipment of the integrated energy system, along with the variation curves of electrical balance, thermal balance, and new energy in EP.

Figure 7 shows that the IES's electrical storage charges from 1:00 to 10:00 and discharges during peak use (10:00–13:00), and resumes charging after 20:00. Thermal storage maintains stability for reliable heat supply. At 19:00, flexible electrical demand is reduced, and multi-energy scheduling helps mitigate shortfalls through load shifting. The thermal balance at 19:00 shows cross-subsystem collaboration to alleviate thermal pressure. The output of renewable energy exhibits distinct peak periods: photovoltaic generation peaks between 8:00 and 18:00, while wind power peaks from 14:00 to 22:00. Load demand also shows specific peaks, with electrical load peaking during 5:00–9:00 and 18:00–21:00, and thermal load peaking at 2:00, 17:00, and 22:00. Energy storage is crucial for load smoothing. Wind power's variability means that reliable thermal storage is needed during thermal load peaks to ensure heating, highlighting the system's resilience.

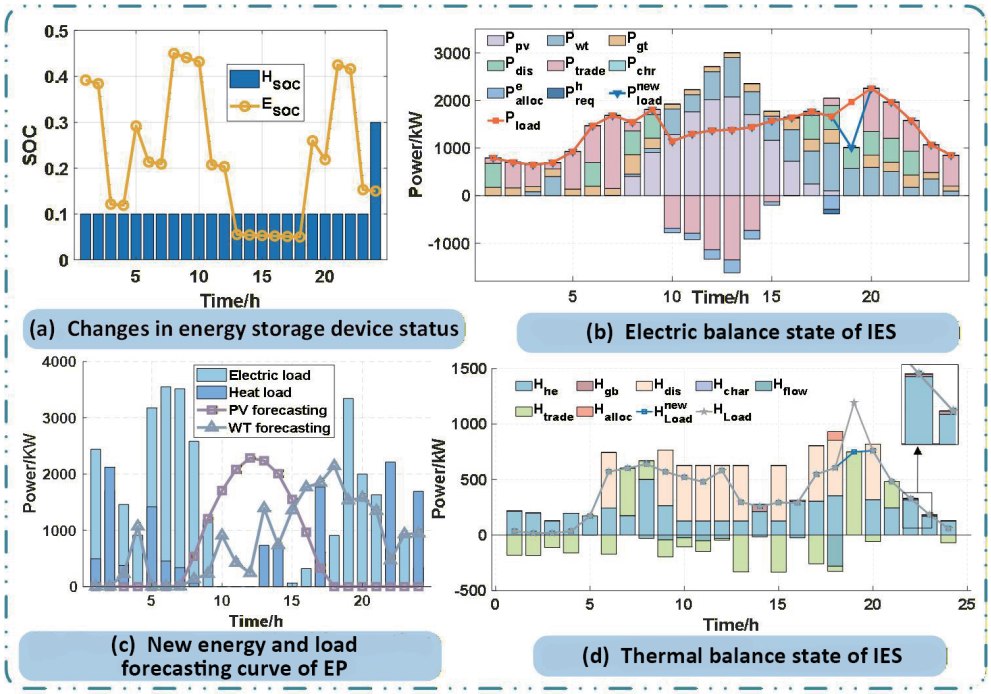

Fig. 7. (Color online) Changing curves of different situations.

As observed in Fig. 7 during the thermal load peak at 19:00, cross-energy compensation is not a simple energy substitution but a systematic flexibility support mechanism. This process is governed by energy conversion efficiencies ($\eta_{e\to h}$ and $\eta_{e\to c}$), defined as the ratio of useful thermal (or cooling) energy output to electrical energy input. The decision to convert electrical energy into heating or cooling energy at an extreme load moment T, such as 19:00 in Fig. 7, follows a structured, cost-driven optimization logic embedded within the scheduling model. A high conversion efficiency acts as a flexibility multiplier. For instance, when $\eta_{e\to h} = 3.5$, 1 kW of electrical flexibility can mitigate a 3.5 kW thermal load deficit. This significantly enhances the system's persistence elasticity, enabling it to maintain operation under extreme loads for a longer duration.

In conclusion, through the implementation of the multi-energy flexibility and multi-time-scale cooperative scheduling strategy—enabling spatiotemporal load transfer, energy storage peak regulation, and cross-subsystem collaboration—the system maintains stable operation under extreme loads, thereby enhancing overall collaborative efficiency.

6. Conclusions

In this study, we addressed the challenges faced by RIES in multi-time-scale collaborative scheduling and response to singular large loads, proposing a comprehensive solution. The main research conclusions are as follows.

- A multi-time-scale collaborative scheduling framework for multi-energy flexibility is proposed. A collaborative scheduling framework for electricity, thermal, and cold energy has been constructed. This framework establishes a dynamic priority mechanism that accounts for peak-valley load differences and energy transmission delays, facilitating multi-time-scale coordination. In extreme load scenarios, a conversion mechanism that transforms electrical energy into thermal and cooling energy provides emergency cross-energy support, significantly enhancing system resilience. The results indicate a 9.1% reduction in operating costs, a 9.9% decrease in carbon emissions, and a 23.9% decline in gas costs.
- An improved MGWCA is developed, which effectively addresses the premature convergence issue of the original algorithm by introducing an elite collaborative strategy and crowding distance sorting. Case 1 validates that MGWCA outperforms the original GWCA concerning the uniformity distribution metric on the ZDT3 function, with an increase of 81.4%. Additionally, it optimizes the operating cost of IES to 882.2$ in real scheduling problems, achieving a reduction of 38.1 to 51.9% compared with benchmark algorithms, demonstrating superior solution performance and stability.
- The strategy adaptability across different scenarios is analyzed. A comparative analysis of scenarios with high and medium proportions of renewable energy integration validates that the proposed strategy can maintain stable system operation across various renewable penetration rates, showcasing good robustness and practicality.
- Furthermore, the pivotal role of multi-source sensing information as the foundation of the proposed framework is underscored. The pervasive deployment of sensors across RIES provides the critical real-time data on renewable energy output, load fluctuations, and

equipment operational status. This high-fidelity data stream is indispensable for the accuracy of day-ahead forecasts, the timeliness of intraday rolling adjustments, and the precision of real-time feedback corrections. Ultimately, it is this sensor-enabled situational awareness and closed-loop control that allows the dynamic priority mechanism and cross-energy support to function effectively, ensuring the system's enhanced economic efficiency, low-carbon performance, and operational resilience under the stress of a single large load.

It is important to reaffirm that the reported optimization improvements—including the 9.1% reduction in operating costs, the 9.9% decrease in carbon emissions, and the 23.9% decline in gas costs—are fundamentally underpinned by the multi-source sensing information-driven approach. The pervasive sensor network provides the essential data fidelity and timeliness required for the accurate state awareness, forecasting, and closed-loop control that define the proposed collaborative scheduling framework.

However, this study's model rests on the assumption of fully reliable sensor data, which may diverge from real-world complexities where data packet loss, communication delays, and sensor faults can occur. Therefore, addressing the uncertainties and reliability of sensor data themselves presents a critical direction for future work. Subsequent research will focus on constructing a stochastic robust optimization model that explicitly considers multi-source data uncertainties, alongside exploring a distributed parallel computing framework to enhance the algorithm's practical application and scalability in ultralarge-scale RIES engineering contexts.

Acknowledgments

This work was supported by the project of Research and Application of Reliability Indicator System Under New Power Systems (No. YNKJXM20240586).

Appendix A

Table A1
Key equipment parameters.

Equipment	Capacity (kW)	Running cost ($/kW)	Efficiency	Charge/discharge power (kW)	Reference
Photovoltaic	2500	0.009	—	—	(16)
Wind turbine	1500	0.015	—	—	(16)
Gas turbine	1000	0.05	0.35 (electrical)	—	(2)
Gas boiler	500	0.075	0.90	—	(15)
Electric chiller	800	—	—	—	(15)
Electrical storage	1200 (kWh)	0.008	0.95	250	(2)
Thermal storage	1000 (kWh)	0.18	0.90	200	(16)

References

1 D. Dwivedi, K. V. S. M. Babu, P. K. Yemula, P. Chakraborty, and M. Pal: Appl. Energy **380** (2025) 125001. https://doi.org/10.1016/j.apenergy.2024.125001
2 Z. F. Liu, S. X. Zhao, X. F. Luo, Y. H. Huang, R. Z. Gu, J. X. Li, and L. L. Li: Appl. Energy **379** (2025) 124918. https://doi.org/10.1016/j.apenergy.2024.124918
3 Z. C. Chen and C. M. Li: Energy **322** (2025) 135491. https://doi.org/10.1016/j.energy.2025.135491

4 Y. Jin, E. Oko, J. Zhang, and J. shen: Energy **313** (2024) 134128. https://doi.org/10.1016/j.energy.2024.134128
5 Y. Li, Z. Pu, P. Liu, T. Qian, Q. Hu, J. Zhang, and Y. Wang: Renew. Energy **240** (2025) 122154. https://doi.org/10.1016/j.renene.2024.122154
6 W. Zhao, W. Chang, and Q. Yang: Renew. Energy **235** (2024) 121363. https://doi.org/10.1016/j.renene.2024.121363
7 Q. Li, Y. Zhou, F. Wei, S. Li, Z. Wang, J. Li, G Zhou, J. Liu, P. Yan, and D. Yu: Appl. Energy **362** (2024) 122980. https://doi.org/10.1016/j.apenergy.2024.122980
8 T. Wang, G. Hu, S. Cho, S. W. Tan, and K. L. Chiang: Energy **328** (2025) 135998. https://doi.org/10.1016/j.energy.2025.135998
9 A. Fathy: Energy **330** (2025) 136963. https://doi.org/10.1016/j.energy.2025.136963
10 Q. Lu, Q. Guo, and W. Zeng: Energy **252** (2022) 124063. https://doi.org/10.1016/j.energy.2022.124063
11 Y. Wu, C. Wang, and Y. Wang: Energy **302** (2024) 131728. https://doi.org/10.1016/j.energy.2024.131728
12 L. L. Wang, R. C. Xian, P. H. Jiao, X. H. Liu, Y. W. Xing, and W. Wang: Energy **288** (2024) 129868. https://doi.org/10.1016/j.energy.2023.129868
13 L. Li, S. Fan, L. Dong, R. Huang, Y. Shen, and G. He: Energy **330** (2025) 136896. https://doi.org/10.1016/j.energy.2025.136896
14 M. Wang, H. Zhao, C. Liu, D. Ma, Y. Jiang, and F. Yang: Appl. Energy **380** (2025) 125071. https://doi.org/10.1016/j.apenergy.2024.125071
15 Z. F. Liu, X. F. Luo, X. R. Chen, Y. H. Huang, Y. Y. Liu, T. Yu, K. Qing, and G. Liang: Renew. Sustain. Energy Rev. **237** (2024) 121682. https://doi.org/10.1016/j.renene.2024.121682
16 Z. F. Liu, X. F. Luo, X. X. Hou, J. L. Yu, and J. X. Li: Renew. Sustain. Energy Rev. **217** (2025) 115752. https://doi.org/10.1016/j.rser.2025.115752
17 Z. Guan, C. Ren, J. Niu, P. X. Wang, and Y. Z. Shang: Expert Syst. Appl. **233** (2023) 120905. https://doi.org/10.1016/j.eswa.2023.120905